Nanoscale

RSC Publishing

PAPER

View Article Online
View Journal | View Issue

Cite this: *Nanoscale*, 2013, **5**, 11686

Efficient and stable $CH_3NH_3PbI_3$-sensitized ZnO nanorod array solid-state solar cells

Dongqin Bi,[a] Gerrit Boschloo,[a] Stefan Schwarzmüller,[b] Lei Yang,[a] Erik M. J. Johansson[a] and Anders Hagfeldt*[a]

Received 28th March 2013
Accepted 3rd September 2013

DOI: 10.1039/c3nr01542d

www.rsc.org/nanoscale

We report for the first time the use of a perovskite ($CH_3NH_3PbI_3$) absorber in combination with ZnO nanorod arrays (NRAs) for solar cell applications. The perovskite material has a higher absorption coefficient than molecular dye sensitizers, gives better solar cell stability, and is therefore more suited as a sensitizer for ZnO NRAs. A solar cell efficiency of 5.0% was achieved under 1000 W m^{-2} AM 1.5 G illumination for a solar cell with the structure: ZnO NRA/$CH_3NH_3PbI_3$/spiro-MeOTAD/Ag. Moreover, the solar cell shows a good long-term stability. Using transient photocurrent and photovoltage measurements it was found that the electron transport time and lifetime vary with the ZnO nanorod length, a trend which is similar to that in dye-sensitized solar cells, DSCs, suggesting a similar charge transfer process in ZnO NRA/$CH_3NH_3PbI_3$ solar cells as in conventional DSCs. Compared to $CH_3NH_3PbI_3$/TiO_2 solar cells, ZnO shows a lower performance due to more recombination losses.

Introduction

Dye-sensitized solar cells (DSCs) have been recognized as one of the most promising alternatives to conventional silicon solar cells.[1,2] As they combine the advantages of low-cost, high-throughput, and low-tech fabrication techniques, they have been shown to be much more competitive in terms of cost, energy-payback time and environmental impact. Recently, DSCs with a liquid redox electrolyte have been developed containing one-electron cobalt-complex redox mediators, with a record efficiency (η) up to 12.3%.[3,4] However, it would be more practical to replace liquid electrolytes with noncorrosive, nonvolatile materials to eradicate most problems related to manufacturing and production lifetime.[5]

To date, the efficiency of solid-state DSCs (ssDSCs) is still lower than the conventional DSCs based on a liquid electrolyte.[6] Generally, the lower performance of ssDSCs is attributed to incomplete pore-filling of the mesoporous TiO_2 with the solid hole transporting material (HTM) and to limited light harvesting because of the use of relatively thin mesoporous TiO_2 films.[7,8] One approach to improve the filling sensitized films with solid HTMs is to replace the nanoparticles in the mesoporous film with vertically ordered (1D) nanostructures, providing a direct pathway for electron transport and a straight channel for filling the pores of the sensitized film with the HTM solution.[9] Among the 1D nanostructures, vertically aligned ZnO nanorod arrays have attracted considerable interest because of their unique material properties as well as easy availability.[10] In particular, single crystalline ZnO nanowires enable fast electron transport and have been used for ssDSCs.[11,12] Gao *et al.* reported efficiencies of 1.7% and 5.65% by using 12 μm and 50 μm multilayers of ZnO nanorod arrays.[9,13] Usually, ZnO nanorod arrays are much shorter (less than 1 μm) and the reported efficiencies are less than 1%.[11,12,14,15] This can be attributed to the insufficient area for dye adsorption, and also aggregation of dye molecules in the ZnO surface and formation of Zn^{2+}–dye complexes, which retards electron injection from the dye to the semiconductor.[16,17] Therefore, using inorganic sensitizers may be a good alternative for ZnO NRA solar cells.[18,19] Kim *et al.* investigated P3HT/CdSe/CdS/ZnO NRA solar cells, and obtained an efficiency of 1.5%.[20] In Table 1, the reported solar cell performance of solid state ZnO NRA solar cells is shown.[9,11–13,15,18–23]

Using $CH_3NH_3PbI_3$ as a sensitizer appears to be a promising way to achieve better efficiency in ZnO NRA based solar cells. The lead perovskite material has a direct band gap, a large absorption coefficient (1.5×10^4 cm^{-1} at 550 nm) and a high carrier mobility, which make it very attractive as a light harvester in heterojunction solar cells.[24,25] Recently, $CH_3NH_3PbI_3$ was applied in hybrid solar cells where it was found to act as a sensitizer,[24] as an electron conductor,[25] and as a hole conductor.[26] Many questions related to charge transport and detailed structures at the interface are still open.[25] In this paper, we report on an easy processable spiro-MeOTAD/$CH_3NH_3PbI_3$/ZnO NRA solar cell, and compare the effect of the nanorod length on the solar cell performance. Furthermore, we investigate the electron transport and recombination processes and the long-term stability of such devices.

[a]*Department of Chemistry – Ångström Laboratory, Physical Chemistry, Uppsala University, Sweden. E-mail: anders.hagfeldt@kemi.uu.se*

[b]*Department Chemie, Ludwig-Maximilians-Universität München, Germany*

Table 1 Performance of solid-state solar cells based on ZnO nanorod arrays

Device structure [reference]	NRA length	η/%	V_{oc}/V	J_{sc}/mA cm^{-2}	FF
Spiro-MeOTAD/D102/ZnO NRAs[12]	600 nm	0.093	0.47	0.73	—
Spiro-MeOTAD/D102/ZnO–MgO/NRAs[12]	600 nm	0.156	0.49	1.12	—
Spiro-MeOTAD/D102/ZnO–ZrO_2/NRAs[12]	600 nm	0.283	0.47	2.14	—
Spiro-MeOTAD/D149/ZnO NRAs[12]	600 nm	0.088	0.47	0.71	—
Spiro-MeOTAD/D149/ZnO–MgO/NRAs[12]	600 nm	0.278	0.58	1.53	—
Spiro-MeOTAD/D149/ZnO–ZrO_2/NRAs[12]	600 nm	0.596	0.57	3.02	—
P3HT/CdS/ZnO NRAs[20]	800 nm	0.24	0.34	1.6	0.43
P3HT/CdSe/CdS/ZnO NRAs[20]	800 nm	1.5	0.675	4.2	0.52
P3HT/N3/ZnO NRAs[21]	250 nm	0.13	0.46	0.72	0.38
P3HT/Z907/ZnO NRAs[15]	110 nm	0.2	0.30	1.73	0.39
P3HT/Z907/ZnO NRAs[22]	500 nm	0.2	0.23	2.0	—
MEH-PPV/Z907/ZnO NRAs[11]	170 nm	0.61	0.29	6.53	0.32
P3HT/mercurochrome/ZnO NRAs[23]	300 nm	0.13	0.34	0.91	0.43
P3HT/CdS/ZnO[18]	180 nm	0.11	0.60	0.39	0.48
MEH-PPV/CdS/ZnO NRAs[19]	200–300 nm	0.65	0.78	2.87	0.29
CuSCN/N719/ZnO NRAs[13]	11–12 μm	1.7	0.57	8.0	—
Spiro-MeOTAD/Z907/ZnO NRAs-TiO_2[9]	50 μm	5.65	0.788	12.2	0.51

Experimental

Fluorine-doped tin oxide (FTO)-coated glass (Pilkington TEC15, 15 Ω □$^{-1}$) was coated with ZnO colloids as described elsewhere, providing a seeding layer for the growth of the ZnO nanorods as well as an electronic blocking underlayer. A solution of $Zn(NO_3)_2 \cdot 6H_2O$ (0.025 M), polyethylenimine (branched) (3 mM) and hexamethylenetetramine (HMTA) (0.025 M) in distilled water[27] was used for hydrothermal growth of the nanorods. A beaker containing this solution was placed with FTO substrates facing down in an oil bath maintained at 85 °C during the whole growth process.[27] The perovskite sensitizer $CH_3NH_3PbI_3$ was prepared according to the reported procedure.[24] Hydroiodic acid (30 mL, 57 wt% in water) was stirred with methylamine (27.8 mL, 0.273 mol, 40% in methanol) at 0 °C for 2 h. The resulting solution was evaporated and the resulting methylammonium iodide (CH_3NH_3I) was readily available for further processing. To prepare $CH_3NH_3PbI_3$, equal molar amounts of CH_3NH_3I and PbI_2 were mixed in γ-butyrolactone at 60 °C and stirred overnight. The ZnO nanorod array substrates were sintered in air at 400 °C for 30 minutes. A 40 wt% perovskite precursor solution was dispensed onto the ZnO nanorod array film *via* spin-coating at 1500 rpm for 30 seconds, followed by heating at 100 °C for 10 min on a hot-plate. The composition of the spin-coating solution for the hole transport material (HTM) was 0.170 M 2,2′,7,7′-tetrakis-(*N*,*N*-di-*p*-methoxyphenyl-amine)-9,9′-spirobifluorene (spiro-MeOTAD), 0.064 M bis(trifluoromethane)sulfonimide lithium salt (LiTFSI) and 0.198 M 4-tert-butylpyridine (TBP) in chlorobenzene. The $CH_3NH_3PbI_3$-sensitized ZnO films were coated with the HTM solution using a spin-coating method at 4000 rpm. A silver contact with a thickness of 200 nm was deposited onto the solar cell by thermal evaporation.

Current–voltage (*J*–*V*) characteristics were measured using a Keithley 2400 source per meter and a Newport solar simulator (model 91160) giving light with AM 1.5 G spectral distribution, which was calibrated using a certified reference solar cell (Fraunhofer ISE) at an intensity of 1000 W m^{-2}, or with the help of a neutral density filter at 100 W m^{-2}. A black mask (0.2 cm^2) was applied on top of the cell to avoid significant additional contribution from light falling on the device outside the active area.

Incident photon to current conversion efficiency (IPCE) spectra were recorded using a computer-controlled setup consisting of a xenon light source (Spectral Products ASBXE-175), a monochromator (Spectral Products CM110), and a Keithley 2700 Multimeter, and calibrated using a certified reference solar cell (Fraunhofer ISE). The electron lifetime and transport time were measured using a white LED (Luxeon Star 1W) as the light source. Voltage and current traces were recorded with a 16-bit resolution digital acquisition board (National Instruments) in combination with a current amplifier (Stanford Research Systems SR570) and a custom-made system using electromagnetic switches.

The cross-sections of the solar cell devices were imaged using a scanning electron microscope (SEM). Samples were scribed on the substrate (glass) side and cracked prior to acquisition of the SEM-images (Zeiss LEO1550 high resolution SEM). The acceleration voltage (EHT) was 10 kV and the working distance (WD) ranged from 12 to 13.5 mm. Entire cross-sections were imaged at a magnification of 50 000.

Results and discussion

In Fig. 1, cross-sectional scanning electron microscopy (SEM) images of the ZnO nanorod array samples are shown. Fig. 1a–f show the bare ZnO nanorod samples obtained at different reaction times. The thickness of the nanorod array layer varied between 400 nm and 1400 nm, while the diameter of the nanorods was almost constant (~50 nm). Upon longer growth of the ZnO nanorod array, the orientation of the rod becomes more perpendicularly aligned with respect to the substrate. Fig. 1g–l show the samples after deposition of $CH_3NH_3PbI_3$ and

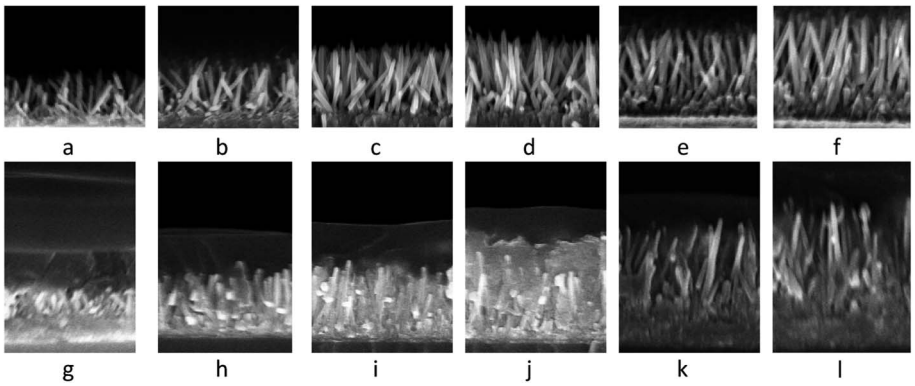

Fig. 1 SEM images of ZnO nanorod arrays (a–f) and spiro-MeOTAD/$CH_3NH_3PbI_3$/ZnO nanorod array samples (g–l) (400 nm).

spiro-MeOTAD. The ZnO NRA appears to be unaffected by the deposition. It can be seen that $CH_3NH_3PbI_3$ effectively penetrates into the interspaces of the ZnO nanorod arrays. The degree of filling can be controlled by varying the concentration of the spin-coating solution.[28] If the concentration is very high, a large degree of filling will be found, and the formation of a capping layer on top of the filled structure by the excess material is expected.[25] For the $CH_3NH_3PbI_3$/ZnO nanorod array electrodes investigated here, however, there was no evidence for the existence of a significant capping layer of the lead perovskite material. Also visible on the SEM images is the HTM spiro-MeOTAD, which forms a capping layer of about 400 nm on top of the $CH_3NH_3PbI_3$/ZnO NRA structure. It is not clear whether the spiro-MeOTAD infiltrates into the $CH_3NH_3PbI_3$/ZnO nanorod structure, but this is expected to occur if some porosity is remaining after $CH_3NH_3PbI_3$ deposition.

UV-Vis spectra of $CH_3NH_3PbI_3$/ZnO nanorod samples show a broad absorption spectrum ranging from 400 nm to 800 nm, see Fig. 2. The absorbance increased with the length of the nanorods, indicating that more of the organic lead perovskite material is deposited. This is in agreement with the SEM analysis.

Fig. 3 shows the effect of the ZnO nanorod length on the key photovoltaic performance parameters of spiro-MeOTAD/$CH_3NH_3PbI_3$/ZnO nanorod array solar cells. The short-circuit current density (J_{sc}), fill factor (FF) and power conversion efficiency (η) first increase and then decrease, the open circuit voltage (V_{oc}) decreases steadily with increasing nanorod length. This trend is similar to that described for ZnO NRA/CdS/CdSe solar cell devices, the difference is that the J_{sc} in the perovskite solar cell is roughly 3 times higher than that in the CdS/CdSe system (J_{sc} = 4.23 mA cm^{-2}).[20] J_{sc} is strongly dependent on the nanorod length; it increases from 8.9 to 12.7 mA cm^{-2} as the nanorod length increases from 400 to 1000 nm. This can be attributed to the higher light harvesting efficiency since a larger amount of $CH_3NH_3PbI_3$ was loaded into the ZnO nanorod structure as the ZnO surface area increased (Fig. 1b). However, after reaching a maximum of 12.7 mA cm^{-2}, J_{sc} decreases slightly. This may be caused by the increased recombination of charges before collection at the contacts, as will be discussed later. The V_{oc} decreased from 0.75 V to 0.42 V as the nanorod length increased from 400 nm to 1400 nm. This strong dependence of V_{oc} on the nanorod length can be attributed to the larger interfacial area: this gives rise to the increased charge separation (and hence photocurrent), but also to increased recombination. The latter dominates at ZnO nanorod lengths larger than one micrometer.

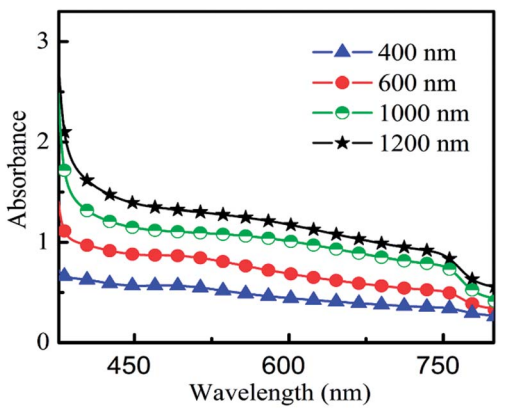

Fig. 2 UV-Vis spectra of $CH_3NH_3PbI_3$/ZnO nanorod array samples. A bare FTO substrate was used as the reference.

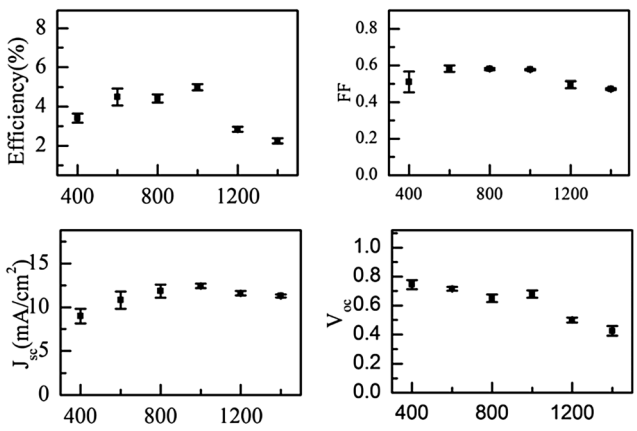

Fig. 3 Effect of ZnO nanorod length (nm) on the key photovoltaic performance parameters of spiro-MeOTAD/$CH_3NH_3PbI_3$/ZnO nanorod array solar cells.

The *J–V* curve of our best spiro-MeOTAD/$CH_3NH_3PbI_3$/ZnO nanorod solar cell is shown in Fig. 4. The top efficiency was 5.0% under 1000 W m^{-2} AM 1.5 G illumination with a J_{sc} of 12.7 mA cm^{-2}, a V_{oc} of 0.68 V and a fill factor of 0.58. At 10% of this light intensity an efficiency of 5.2% was recorded. Note that the V_{oc} and J_{sc} values found here are much higher than typical values for dye-sensitized ZnO nanorod array solar cells with a rod length ranging between 200 nm and 1800 nm (V_{oc} = 0.25–0.59 V, J_{sc} = 0.31–2.0 mA cm^{-2}).[14,22] The $CH_3NH_3PbI_3$/ZnO nanorod system exhibits a broad IPCE spectrum from 400 to 800 nm with maximum values above 60% in the wavelength range of 400–540 nm (Fig. 2), which is much better than comparable values found in ssDSCs based on ZnO nanorod arrays.[11,22]

The light intensity dependence of J_{sc} and V_{oc} was investigated in the $CH_3NH_3PbI_3$/ZnO nanorod devices, see Fig. 5a and b. A linear dependence of J_{sc} on incident light intensity I is found (the fit of $J_{sc} \propto I^{\alpha}$ yielded $\alpha = 1.0$), which is typical for well-behaved solar cells. The slope in V_{oc} *versus* intensity varied slightly with the nanorod length: it was about 170 mV per decade for 600 nm and 1.0 μm, and 118 mV per decade for 1.4 μm length. Notably, it is significantly higher than the value of 59 mV per decade that is expected in dye-sensitized solar cells, when recombination of a conduction band electron from the metal oxide to the redox electrolyte shows first order kinetics. It seems to be a reasonable approximation that the doping level of the spiro-MeOTAD does not change much when the light intensity is varied, and that the Fermi level in the HTM can be considered as a constant. Deviation from the first order recombination kinetics can be attributed to trap-assisted recombination, inhomogeneous recombination due to the variations in the thickness of the $CH_3NH_3PbI_3$ absorber, as well as from a poor blocking layer at the FTO contact.

Photovoltage transient measurements under open-circuit conditions were used to determine the electron lifetime (τ_e) in DSCs. The measured τ_e is shown as a function of V_{oc} (Fig. 5c). As expected, τ_e decreases with increasing V_{oc} (and increasing light intensity). Moreover, the nanorod length affects the lifetime very strongly. The lifetime values in Fig. 5d are similar to those found in comparable ssDSCs,[11] indicating that the enhanced solar cell performance found here mainly comes from the enhanced light harvesting. For optimized solar cell performance, a ZnO nanorod length of about 800 nm is sufficient: longer nanorods do not lead to significantly more light harvesting (note that the devices have a reflective metal back contact), but does lead to significantly faster electron–hole recombination.

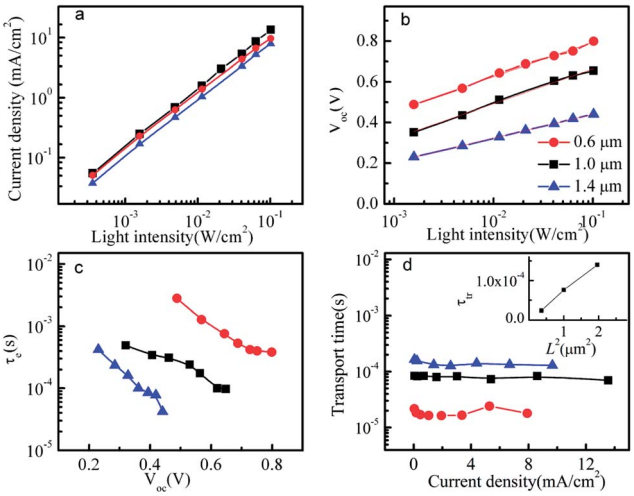

Fig. 5 The light intensity dependence of J_{sc} (a) and V_{oc} (b), electron lifetime as a function of open circuit voltage (c) and transport time as a function of current density (d) in the spiro-MeOTAD/$CH_3NH_3PbI_3$/ZnO solar cell. The inset of (d) shows the electron transport time as a function of L^2 (L: nanorod length).

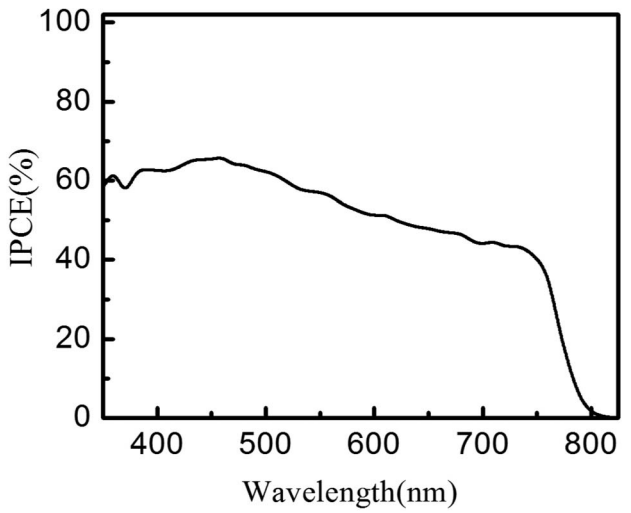

Fig. 4 *J–V* curve under AM 1.5 G illumination of 1000 W m^{-2} and 100 W m^{-2}, and spectra of incident photon to current efficiency (IPCE) of a spiro-MeOTAD/$CH_3NH_3PbI_3$/ZnO solar cell.

Photocurrent response times were determined under short-circuit conditions using small square wave modulation of the light intensity, see Fig. 5d. We attribute the photocurrent response time to the electron transport time (t_{tr}) in the ZnO nanorods, as the HTM is highly doped. Interestingly, the dynamics of electron transport are insensitive to light intensity, which differs from the typical enhancement of transport dynamics with increasing light intensity in traditional DSCs. In that case, it is assumed that most electrons are trapped in states that are distributed over a range of energies. Electron transport is thought to occur by thermal detrapping, followed by rapid movement through the conduction band until the next trapping event and the electron is largely immobilized.[29] Multiple trapping/detrapping does not seem to occur in the ZnO NRA, which may be attributed to the fact that each nanorod is a single crystal. Similar results for ZnO NRAs in DSCs have been reported before.[30] The inset of Fig. 5d shows that the transport time scales with the square of the nanorod length, suggesting that electron transport occurs by diffusion. Using $D = L^2/(2.47t_{tr})$, an electron diffusion coefficient (D) of 5.4 × 10^{-5} cm^2 s^{-1} is calculated, which is much lower than expected for electron diffusion in a ZnO single crystal.[31]

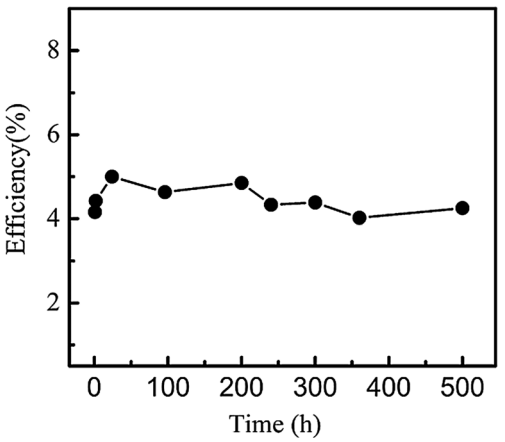

Fig. 6 Efficiency of a $CH_3NH_3PbI_3$/ZnO nanorod solar cell as a function of storage time. The device was stored under lab conditions and measured at 1 sun.

The t_{tr} and τ_e dependence on the nanorod length is similar to that in DSCs based on ZnO NRAs,[30] indicating that the injected electrons are transported though the ZnO nanorod, which is different from the reported $Al_2O_3/CH_3NH_3PbI_2Cl$ solar cell where electron transport occurs in the perovskite layer.[25] The electron transport time in the ZnO NRAs is slightly faster than that in mesoporous TiO_2 films of similar thickness.[25] The spiro-MeOTAD/$CH_3NH_3PbI_3$/ZnO nanorod solar cells show lower performance compared to similar devices with mesoporous TiO_2 as the metal oxide. The difference mainly stems from the difference in V_{oc}, being about 200 mV higher in TiO_2-based devices. This is surprising, since TiO_2 (anatase) and ZnO are expected to have a similar conduction band edge potential. In DSCs similar V_{oc} values are indeed found.[32] Origin of the lower V_{oc} seems to be the relatively fast recombination in ZnO NRA/perovskite solar cells, which is most evident for the devices with relatively long nanorods.

The stability of spiro-MeOTAD/$CH_3NH_3PbI_3$/ZnO nanorod devices was investigated by storing them in air at room temperature without further encapsulation. At selected times, the devices were characterized under 1000 W m^{-2} AM1.5 illumination, see Fig. 6. After 500 hours of storage the overall conversion efficiency was only slightly decreased from a maximum value of 5.0% to 4.35%. This result is much better than previous reports on stability of DSCs based on ZnO nanostructures.

Conclusions

In conclusion, a spiro-MeOTAD/$CH_3NH_3PbI_3$/ZnO nanorod array solar cell was developed and characterized in this report. The ZnO nanorods offer a fast electron transport pathway and the $CH_3NH_3PbI_3$ results in efficient visible light harvesting. The optimized solar cell exhibited an efficiency of 5.0% under 1000 W m^{-2} AM1.5 illumination. The fabricated perovskite solar cell exhibited promising initial stability. The better solar cell performance compared to other solar cells based on ZnO nanorod arrays is attributed to the enhanced light harvesting. The dependence of the electron transport and recombination on the nanorod length is similar to that found in dye-sensitized solar cells based on ZnO NRAs. Compared to $CH_3NH_3PbI_3/TiO_2$ solar cells, ZnO shows a lower performance due to more recombination losses.

Acknowledgements

We thank the Swedish Energy Agency, the Swedish Research Council (VR), the Göran Gustafsson Foundation, the STandUP for Energy program, and the Knut and Alice Wallenberg Foundation for financial support.

References

1 A. Hagfeldt, G. Boschloo, L. Sun, L. Kloo and H. Pettersson, *Chem. Rev.*, 2010, **110**, 6595–6663.
2 B. O'Regan and M. Gratzel, *Nature*, 1991, **353**, 737–740.
3 A. Yella, H. W. Lee, H. N. Tsao, C. Y. Yi, A. K. Chandiran, M. K. Nazeeruddin, E. W. G. Diau, C. Y. Yeh, S. M. Zakeeruddin and M. Gratzel, *Science*, 2011, **334**, 629–634.
4 S. M. Feldt, E. A. Gibson, E. Gabrielsson, L. Sun, G. Boschloo and A. Hagfeldt, *J. Am. Chem. Soc.*, 2010, **132**, 16714–16724.
5 U. Bach, D. Lupo, P. Comte, J. E. Moser, F. Weissortel, J. Salbeck, H. Spreitzer and M. Gratzel, *Nature*, 1998, **395**, 583–585.
6 J. Burschka, A. Dualeh, F. Kessler, E. Baranoff, N.-L. Cevey-Ha, C. Yi, M. K. Nazeeruddin and M. Grätzel, *J. Am. Chem. Soc.*, 2011, **133**, 18042–18045.
7 P. Docampo, A. Hey, S. Guldin, R. Gunning, U. Steiner and H. J. Snaith, *Adv. Funct. Mater.*, 2012, 1–10.
8 L. Schmidt-Mende, S. M. Zakeeruddin and M. Gratzel, *Appl. Phys. Lett.*, 2005, **86**, 013504.
9 C. K. Xu, J. M. Wu, U. V. Desai and D. Gao, *Nano Lett.*, 2012, **12**, 2420–2424.
10 D. Q. Bi, F. Wu, W. J. Yue, Y. Guo, W. Shen, R. X. Peng, H. A. Wu, X. K. Wang and M. T. Wang, *J. Phys. Chem. C*, 2010, **114**, 13846–13852.
11 D. Q. Bi, F. Wu, Q. Y. Qu, W. J. Yue, Q. Cui, W. Shen, R. Q. Chen, C. W. Liu, Z. L. Qiu and M. T. Wang, *J. Phys. Chem. C*, 2011, **115**, 3745–3752.
12 N. O. V. Plank, I. Howard, A. Rao, M. W. B. Wilson, C. Ducati, R. S. Mane, J. S. Bendall, R. R. M. Louca, N. C. Greenham, H. Miura, R. H. Friend, H. J. Snaith and M. E. Welland, *J. Phys. Chem. C*, 2009, **113**, 18515–18522.
13 U. V. Desai, C. K. Xu, J. M. Wu and D. Gao, *Nanotechnology*, 2012, **23**, 205401.
14 Y. M. Lee and H. W. Yang, *J. Solid State Chem.*, 2011, **184**, 615–623.
15 A. M. Peiro, P. Ravirajan, K. Govender, D. S. Boyle, P. O'Brien, D. D. C. Bradley, J. Nelson and J. R. Durrant, *J. Mater. Chem.*, 2006, **16**, 2088–2096.
16 J. A. Anta, E. Guillén and R. Tena-Zaera, *J. Phys. Chem. C*, 2012, **116**, 11413–11425.
17 T. Horiuchi, H. Miura, K. Sumioka and S. Uchida, *J. Am. Chem. Soc.*, 2004, **126**, 12218–12219.

18 L. D. Wang, D. X. Zhao, Z. S. Su, B. H. Li, Z. Z. Zhang and D. Z. Shen, *J. Electrochem. Soc.*, 2011, **158**, H804–H807.
19 E. D. Spoerke, M. T. Lloyd, E. M. McCready, D. C. Olson, Y. J. Lee and J. W. P. Hsu, *Appl. Phys. Lett.*, 2009, **95**, 3232231.
20 H. Kim, H. Jeong, T. K. An, C. E. Park and K. Yong, *ACS Appl. Mater. Interfaces*, 2013, **5**, 268–275.
21 T. H. Lee, H. J. Sue and X. Cheng, *Nanoscale Res. Lett.*, 2011, **6**, 517.
22 P. Ravirajan, A. M. Peiro, M. K. Nazeeruddin, M. Graetzel, D. D. C. Bradley, J. R. Durrant and J. Nelson, *J. Phys. Chem. B*, 2006, **110**, 7635–7639.
23 T. H. Lee, H. J. Sue and X. Cheng, *Nanotechnology*, 2011, **22**, 285401.
24 H. S. Kim, C. R. Lee, J. H. Im, K. B. Lee, T. Moehl, A. Marchioro, S. J. Moon, R. Humphry-Baker, J. H. Yum, J. E. Moser, M. Gratzel and N. G. Park, *Sci. Rep.*, 2012, **2**, 591.
25 M. M. Lee, J. Teuscher, T. Miyasaka, T. N. Murakami and H. J. Snaith, *Science*, 2012, **338**, 643–647.
26 L. Etgar, P. Gao, Z. Xue, Q. Peng, A. K. Chandiran, B. Liu, M. K. Nazeeruddin and M. Grätzel, *J. Am. Chem. Soc.*, 2012, **134**, 17396–17399.
27 (*a*) M. Law, L. E. Greene, J. C. Johnson, R. Saykally and P. D. Yang, *Nat. Mater.*, 2005, **4**, 455–459; (*b*) L. E. Greene, M. Law, J. Goldberger, F. Kim, J. C. Johnson, Y. Zhang, R. J. Saykally and P. D. Yang, *Angew. Chem., Int. Ed.*, 2003, **42**, 3031–3034.
28 P. Docampo, A. Hey, S. Guldin, R. Gunning, U. Steiner and H. J. Snaith, *Adv. Funct. Mater.*, 2012, **22**, 5010–5019.
29 A. J. Frank, N. Kopidakis and J. v. d. Lagemaat, *Coord. Chem. Rev.*, 2004, **248**, 1165–1179.
30 E. Galoppini, J. Rochford, H. H. Chen, G. Saraf, Y. C. Lu, A. Hagfeldt and G. Boschloo, *J. Phys. Chem. B*, 2006, **110**, 16159–16161.
31 J. Nissfolk, K. Fredin, J. Simiyu, L. Haggman, A. Hagfeldt and G. Boschloo, *J. Electroanal. Chem.*, 2010, **646**, 91–99.
32 M. Quintana, T. Edvinsson, A. Hagfeldt and G. Boschloo, *J. Phys. Chem. C*, 2006, **111**, 1035–1041.